Research Article

Green Synthesis of Mesoporous TiO_2 Nanoparticles via *Colocasia esculenta* L. Leaf Extract: Influence of Calcination Temperature on Physicochemical Properties

Linda Jati Kusumawardani*, Aisyaharani Putri Winanti and Ani Iryani
Department of Chemistry, Faculty of Mathematics and Natural Sciences, Universitas Pakuan, Bogor 16143, Indonesia

Nurlela Nurlela
Research Center for Pharmaceutical Ingredient and Traditional Medicine, National Research and Innovation Agency (BRIN), Kawasan Sains dan Teknologi (KST) Soekarno, Cibinong, West Java, Indonesia.

I Putu Mahendra
Department of Chemistry, Institut Teknologi Sumatera, Terusan Ryacudu, Way Hui, Jati Agung, Lampung Selatan, Indonesia

Tri Saptari Haryani
Department of Biology, Faculty of Mathematics and Natural Sciences, Universitas Pakuan, Bogor 16143, Indonesia

* Corresponding author. E-mail: linda.wardani@unpak.ac.id DOI: 10.14416/j.asep.2026.04.003
Received: 24 September 2025; Revised: 4 December 2025; Accepted: 26 January 2026; Published online: 7 April 2026

Abstract
TiO_2 nanoparticles were successfully synthesized using *Colocasia esculenta* L. leaf extracts (TiO_2–CELEs) and calcined at various temperatures (300–600 °C). Among the samples, TiO_2–CELEs 400 (400 °C) and TiO_2–CELEs 500 (500 °C) exhibited outstanding photocatalytic activity, achieving nearly complete degradation of methylene blue under light irradiation. TiO_2–CELEs 400 showed the largest surface area (106.31 m^2/g) with well-developed mesopores, resulting in enhanced adsorption capacity. In contrast, TiO_2–CELEs 500 demonstrated superior photocatalytic performance despite its lower surface area, primarily due to its higher crystallinity, which facilitated more efficient charge separation and suppressed electron–hole recombination. X-ray diffraction (XRD) analysis revealed that increasing the calcination temperature enlarged the crystallite size (5.22–18.11 nm) and crystallinity (71.50–82.80%). Diffuse reflectance spectroscopy (DRS) indicated band gap narrowing from 3.25 to 3.10 eV, signifying the onset of the anatase–rutile phase transition. Brunauer–Emmett–Teller (BET) analysis confirmed mesoporous characteristics with an unusual desorption-over-adsorption pattern, suggesting flexible pores that facilitate molecular diffusion. Scanning electron microscopy–energy dispersive X-ray spectroscopy (SEM–EDS) confirmed the morphology and high purity of the nanospheres, with only minor potassium residues from CELEs metabolites. Overall, optimizing the calcination temperature effectively balanced surface area and crystallinity, establishing CELEs as a promising, eco-friendly biotemplate for developing high-performance TiO_2 photocatalysts applicable to photocatalysis, dye–sensitized solar cells, medical and environmental remediation.

Keywords: Calcination temperature, *Colocasia esculenta* L., Green synthesis, Photocatalyst, TiO_2 nanoparticles

1 Introduction

Titanium dioxide (TiO_2) is an n–type semiconductor that has been extensively studied due to its excellent characteristics, such as high thermal stability, biocompatibility, non–toxicity, and favorable optical and dielectric properties. TiO_2 exists in three primary crystalline phases: rutile, brookite, and anatase [1].

Among these, the anatase phase with a particle size of less than 11 nm and a band gap of approximately 3.20 eV is known to be the most active in various photocatalytic and antibacterial applications [2]. TiO_2 nanoparticles are widely used for environmental photocatalysis for pollutant degradation, photoanode materials in dye–sensitized solar cells (DSSC), antibacterial coatings, and self–cleaning surfaces.

Various chemical methods have been developed to synthesize TiO_2 nanoparticles, including sol–gel, hydrothermal, and solvothermal methods [3]. However, these approaches often require expensive and toxic chemicals that can contaminate the environment, leading to ecotoxicological concerns [4]. Therefore, green synthesis, which employs natural reducing agents such as plant extracts, microbes, and enzymes, has emerged as a promising alternative due to its low cost, eco–friendliness, and low toxicity [5]. Plant extracts are rich in secondary metabolites such as polyphenols, terpenoids, saponins, and alkaloids, which can effectively reduce metal ions and stabilize nanoparticle formation [6]. Moreover, green synthesis of TiO_2 nanoparticles using plant extracts offers advantages such as producing smaller particles and providing more active sites, which can enhance photocatalytic activity compared to conventional chemical methods [7]. Studies have shown that green–synthesized nanoparticles are smaller in size, have a larger surface area, and contain more active sites, thereby improving performance in applications such as photocatalysis and antibacterial treatments through the generation of reactive oxygen species (ROS) that damage microbial cell walls [8]–[10].

Our previous studies successfully synthesized TiO_2 nanoparticles via chemical routes for organic waste and dye degradation [11]–[14]. However, for broader biomedical and environmental applications, a greener and more biocompatible approach is essential [15]. Several plant extracts have been studied, including those from moringa leaves, orange jasmine leaves, lemon peel extract, aloe vera, elephant grass leaves, red spinach leaves, soybean extract, menteng fruit peel extract, black plum leaves and bilimbi fruit [10], [16]–[19].

Despite the abundance of phytochemical–rich flora, many local plants remain underexplored for nanoparticle synthesis. One such promising bioresource is *Colocasia esculenta* L. leaves, which are rich in phenolic compounds containing hydroxyl and conjugated carbonyl groups that can act as natural reducing and stabilizing agents during nanoparticle formation [20]. *Colocasia esculenta* L. leaves, rich in phenolic compounds (41 identified phenolics and flavonoids) [21], were extracted using ethanol to obtain a potent bioreducing agent for TiO_2 nanoparticle synthesis. *Colocasia esculenta* L. plants are highly adaptive and grow naturally in humid tropical regions, particularly in lowland areas up to an altitude of around 500 meters above sea level, like in West Java, Indonesia, especially in the Bogor region. *Colocasia esculenta* L is commonly found growing wild as well as cultivated as an ornamental plant, reflecting its ecological abundance and close association with local communities [22].

To date, no scientific study has reported the use of *Colocasia esculenta* L. leaf extract (CELEs) for TiO_2 nanoparticle synthesis, nor has any systematic investigation been conducted on the influence of calcination temperature on the structural and functional properties of green–synthesized TiO_2. Calcination temperature is known to play a crucial role in governing crystallite growth, phase transformation (anatase–to–rutile), and surface area evolution–parameters that directly influence photocatalytic efficiency [23].

To the best of our knowledge, this is the first study to employ CELEs as a green precursor for TiO_2 nanoparticle synthesis while systematically investigating the influence of calcination temperature. The calcination range of 300–600 °C was chosen to optimize phase transformation and thermal stability of TiO_2 nanoparticles. Below 300 °C, organic residues may remain, while temperatures above 600 °C promote grain growth. This range enables anatase–rutile transition with optimal crystallinity and photocatalytic performance [24]. This dual novelty, combining a locally abundant phenolic-rich extract with optimized calcination, effectively bridges two major research gaps: (1) the lack of exploration of *Colocasia esculenta* L. as a sustainable reducing agent and (2) the limited understanding of temperature–driven phase and property evolution in green–synthesized TiO_2. The insights from this work not only advance green synthesis strategies but also contribute to sustainable nanomaterial development for photocatalysis, dye–sensitized solar cells, medical and environmental remediation.

2 Research Method

2.1 *Materials*

Colocasia esculenta L. leaves were collected from a local plantation in Bogor, West Java, Indonesia. Analytical grade chemicals, including titanium tetra–isopropoxide (TTIP), TiO_2 anatase powder (99.8% trace metal basis) as standard, and ethanol, were purchased from Merck Sigma-Aldrich and used without further purification.

2.2 *Instruments*

Diffuse Reflectance Spectroscopy (DRS, Thermoscientific) was employed to evaluate the optical absorption properties and estimate the band gap energy of the samples. The specific surface area, pore volume, and pore size distribution of TiO_2 nanoparticles were determined using the Brunauer–Emmett–Teller (BET) method (Quantachrome Novatouch LX–4). X–ray diffraction (XRD, Bruker D8 Advance) was used to analyze the crystalline phase composition, crystallite size, and degree of crystallinity of TiO_2 nanoparticles. Fourier–transform infrared (FTIR, FT 1000) spectroscopy was applied to identify characteristic chemical bonds and functional groups, confirming the presence of Ti–O–Ti and Ti–O–Si linkages, while scanning electron microscopy-Energy Dispersive X–Ray Spectroscopy (SEM–EDS, SU3500) was conducted to examine the surface morphology and elemental composition of the nanocomposites.

2.3 *Preparation of Colocasia esculenta L. leaf extracts (CELEs)*

Before extract preparation, fresh leaves were thoroughly washed with double–distilled water to remove surface impurities and air–dried at room temperature for 3–5 days, protected from direct sunlight, until a constant weight was achieved. The dried leaves were then ground and sieved to obtain simplicia powder, defined as dried plant material with a particle size of approximately 60–80 mesh. A total of 20 g of simplicia powder was placed in a maceration container, followed by the addition of 200 mL of 96% ethanol (1:20 w/v ratio). The mixture was soaked for 24 hours at room temperature with occasional stirring, then filtered to obtain Filtrate I. The residue was re–macerated with an additional 200 mL of 96% ethanol for 24 hours and filtered to obtain Filtrate II. This maceration process was repeated once more with 200 mL of 96% ethanol for 24 hours to produce Filtrate III. All three filtrates were combined and concentrated using a rotary evaporator at 48 °C, yielding 1.3544 g of a thick ethanolic extract, hereafter referred to as CELEs (*Colocasia esculenta* L. leaf extract).

2.4 *Preliminary phytochemical screening of CELEs by detection of secondary metabolites*

The chemical constituents of CELEs were examined through preliminary qualitative phytochemical screening.

2.4.1 Alkaloid detection

The presence of alkaloids in *Colocasia esculenta* L. leaf extracts (CELEs) was verified using three classic phytochemical tests–Mayer's, Dragendorff's, and Wagner's. Before each test, the extract was first acidified with a mild hydrochloric acid solution (1–2%) to convert alkaloids into their soluble salt forms. In Mayer's test, mixing the extract with Mayer's reagent and gently heating it produced a creamy yellow precipitate, signaling the presence of alkaloids. The Dragendorff's test gave similar confirmation, where adding a few drops of Dragendorff's reagent to the acidified extract yielded an orange to reddish–orange precipitate. Likewise, the Wagner's test produced a reddish–brown precipitate after treatment with iodine–potassium iodide reagent. The consistent formation of these characteristic colors across all three tests clearly indicated that alkaloid compounds were present in the CELEs sample.

2.4.2 Flavonoid detection (Alkaline reagent test)

One milliliter of sodium hydroxide solution was added to 1 mL of CELEs, producing an intense yellow coloration. The solution became colorless upon the addition of diluted hydrochloric acid, indicating the presence of flavonoids.

2.4.3 Phenolic compound detection (Ferric chloride test)

A few drops of ferric chloride solution were added to 1 mL of CELEs, resulting in a deep bluish–green coloration, which confirmed the presence of phenolic compounds.

2.4.4 Saponin detection (Foam test)

A mixture of 1 mL CELEs and 1 mL water was shaken thoroughly. The formation of persistent foam indicated the presence of saponins.

2.4.5 Steroid detection (Liebermann–burchard test)

Steroid screening of CELEs was performed using the Liebermann–Burchard test. Briefly, 1–2 mL of CELEs was dissolved in 1–2 mL of chloroform in a test tube, followed by the addition of 1–2 drops of acetic anhydride with gentle mixing. Subsequently, 1–2 mL of concentrated sulfuric acid was carefully added along the side of the test tube to form a separate layer. The color change at the interface was observed for 1–5 min, where the appearance of a green to bluish-green color indicated the presence of steroids or sterols. As the reagent is highly sensitive and may produce similar reactions with terpenoids, positive controls were used to confirm the results.

2.4.6 Terpenoid detection (Salkowski test)

Terpenoid screening of CELEs was conducted using the Salkowski test. Briefly, 1–2 mL of CELEs was dissolved in 2 mL of chloroform in a test tube, and 2–3 drops of concentrated sulfuric acid were carefully added along the side of the tube to form a separate layer. The color change at the interface was observed, where the development of a reddish–brown coloration at the acid layer indicated the presence of terpenoids.

2.4.7 Tanin detection (Ferric chloride test)

Tannin screening of CELEs was performed using the ferric chloride test. Briefly, 1 mL of CELEs was prepared in aqueous solution, and a few drops of 1–5% ferric chloride solution were added. The formation of a blue–black or greenish–black coloration indicated the presence of hydrolyzable or condensed tannins, respectively.

2.5 *Determination of Total Phenolic Content (TPC)*

The total phenolic content was determined at the Service Laboratory, Faculty of Mathematics and Natural Sciences, Universitas Pakuan, using the Folin–Ciocalteu method.

2.5.1 Preparation of gallic acid standard solution

Gallic acid (10 mg) was dissolved in ethanol in a 20 mL volumetric flask to obtain a 500 ppm stock solution. Serial dilutions were prepared by pipetting 200, 400, 600, 800, and 1000 µL into 5 mL test tubes and adjusting with ethanol to final concentrations of 20, 40, 60, 80, and 100 ppm, respectively. Each standard solution (1 mL) was mixed with 5 mL of 10% Folin–Ciocalteu reagent and allowed to react for 3–8 min, followed by the addition of 4 mL of 7.5% Na_2CO_3 solution. The mixture was homogenized using a vortex, incubated at room temperature for 30 min, and the absorbance was measured at 760 nm using a UV–Visible spectrophotometer. A blank solution was prepared using the same procedure without gallic acid.

2.5.2 Preparation of sample solution

The sample (30 mg) was dissolved in 10 mL of ethanol to obtain a 3000 ppm stock solution. An aliquot of 1 mL was diluted stepwise in a 10 mL volumetric test tube. From this solution, 1 mL was reacted with 5 mL of 10% Folin–Ciocalteu reagent (3–8 min), followed by 4 mL of 7.5% Na_2CO_3. After homogenization with a vortex, the mixture was incubated at room temperature for 30 min, and the absorbance was measured at 760 nm.

2.6 *Green Synthesis of TiO_2–CELEs Nanoparticles*

Titanium(IV) isopropoxide (TTIP, 2 mL) was dissolved in 30 mL of ethanol and stirred for 1 min. Prior to use, a 20 mg extract was dissolved in 96 mL of distilled water to obtain a homogeneous solution. Subsequently, the CELEs solution was added to the TTIP solution at a volumetric ratio of 1:3 (v/v, TTIP:CELEs), corresponding to an equivalent ratio of 32 mL TTIP to 96 mL CELEs solution, under continuous stirring. The mixture was stirred at 300 rpm for 4 h, during which the formation of TiO_2 nanoparticles (TiO_2 NPs) was indicated by a color change from transparent to brown. The reaction mixture was allowed to cool to room temperature and centrifuged at 5000 rpm for 15 minutes to collect the precipitate, which was washed three times with deionized water and ethanol. The resulting TiO_2–CELEs were air–dried at room temperature for 24 h, followed by calcination at varying temperatures of 300, 400, 500, and 600 °C for 3 hours each. The samples, denoted as TiO_2–CELEs x (x = 300–600),

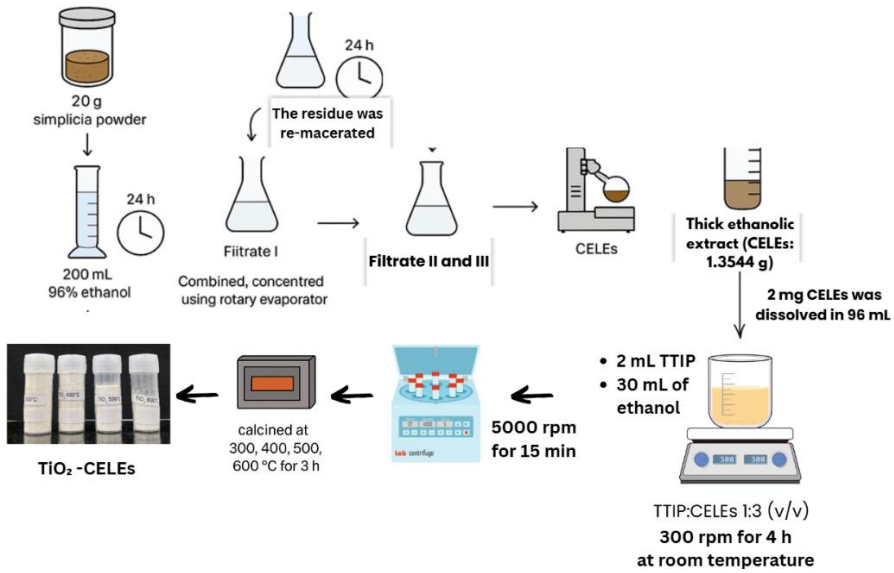

Figure 1: Schematic diagram of TiO_2 nanoparticle synthesis using *Colocasia esculenta* L.

were obtained through calcination at different temperatures. A schematic representation of the CELEs–mediated process for synthesizing TiO_2 nanoparticles is presented in Figure 1.

3 Result and Discussion

3.1 *Initial phytochemical analysis of CELEs*

The preparation of simplicia plays a crucial role in determining the quality of the resulting extract. *Colocasia esculenta* L. leaf simplicia was dried to reduce its moisture content, thereby preventing microbial growth and improving storage stability. Sun–drying was employed to preserve the secondary metabolites in taro leaves and minimize their degradation. The dried simplicia were then pulverized to increase the surface area, thus enhancing the interaction between the sample and the solvent during maceration [25].

In this study, extraction was performed using the maceration method with ethanol as the solvent, followed by concentration with a rotary evaporator. This process yielded a simplicia extract of 6.77% and a total phenolic content of 33.20 mg GAE/g. These values are considerably higher than those reported previously, who employed an extraction method involving stirring and low–temperature heating with water as the solvent and obtained a relatively low phenolic content of 0.65 mg GAE/g [19]. Similarly, another ethanol–based extraction reported a total phenolic content of only about 5 mg GAE/g [26]. In addition, the extract obtained in this study demonstrated good stability, maintaining its physical and chemical properties for up to two months of storage, confirming its suitability as a stable and effective bioreductant source for nanoparticle synthesis.

Table 1: Identification of phytochemical compounds.

No	Tests	Observation
1	Alkaloids	
	Mayer	–
	Wagner	+
	Dragendorff	+
2	Flavonoids	+
3	Steroids and Terpenoids	+
4	Saponins	+
5	Tannins	+

A qualitative phytochemical screening of the ethanol extract of taro leaves confirmed the presence of several secondary metabolites, including alkaloids, flavonoids, saponins, tannins, steroids, and terpenoids (Table 1). Notably, the detection of flavonoids and tannins supports the high total phenolic content obtained in this study (33.20 mg GAE/g), as both

groups are major phenolic constituents. These findings indicate that CELEs are rich in phenolic compounds, which may contribute substantially to their bioactive potential [27]. Prior to use, a 20 mg extract (equivalent to 0.664 mg GAE) was dissolved in 96 mL of distilled water, yielding a concentration of approximately 6.92 ppm. These findings indicate that CELEs are rich in phenolic compounds, which may contribute substantially to their bioactive potential.

3.2 *Green synthesis of TiO_2–CELEs nanoparticles*

The green synthesis approach is simple, safe, cost–effective, and environmentally friendly. In this study, titanium isopropoxide (TTIP) was employed as a precursor, while CELEs served simultaneously as the reducing agent, capping agent, and stabilizer. The secondary metabolites present in CELEs were confirmed through phytochemical screening and total phenolic content analysis [26].

The synthesis procedure began with dissolving the concentrated extract in water, which was subsequently added to a TTIP solution prepared in ethanol. This mixture underwent hydrolysis, in which polyphenols in the extract acted as bioreductants by interacting with Ti^{4+} metal centers, thereby reducing them to Ti^0. During the subsequent three hours of stirring, condensation reactions occurred among the hydroxyl groups (Ti–OH) formed in the process. These condensation reactions generated Ti–O–Ti bridging bonds, leading to the development of a three–dimensional network that served as the basis for gel formation. This step is crucial as it governs the stability, homogeneity, and particle size distribution of the synthesized material [27].

The functional groups in CELEs surrounded the Ti^0 surface, acting as capping agents and imparting a negative surface charge. This negative charge induced electrostatic repulsion between particles, thereby preventing agglomeration and maintaining nanoscale stability [28]. The reaction mechanism involved in the synthesis is illustrated as follows:

$$Ti(OC_3H_7)_4 + 4H_2O \rightarrow Ti(OH)_4 + 4C_3H_7OH$$
$$2Ti(OH)_4 \rightarrow 2TiO \cdot xH_2O + (2 - x)H_2O$$
$$2TiO \cdot xH_2O \rightarrow 2TiO + xH_2O$$

Subsequent steps involved separation and drying processes. First, the nanoparticles were separated from the solvent by centrifugation. This was followed by an aging stage, in which the material was oven–dried overnight (approximately 16 h) at 80 °C to remove residual water molecules. During the aging process, further polycondensation among hydroxyl groups strengthened the gel network, reduced porosity, and enhanced the structural integrity of the gel. As shown in Figure 2, these treatments were also accompanied by a distinct color transition: the TiO_2 nanoparticles initially appeared yellowish–white (Figure 2(a)), turned greenish after oven–drying (Figure 2(b)), and finally became bright white following calcination (Figure 2(c)), reflecting the progressive structural transformation of the material.

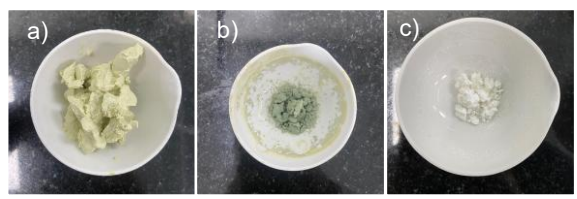

Figure 2: TiO_2 NPs (a) before oven, (b) after oven, (c) after calcination.

Thereafter, a calcination step was carried out, in which amorphous TiO_2 was converted into its crystalline forms (anatase or rutile). Calcination was performed at different temperatures, specifically 300, 400, 500, and 600 °C. By applying calcination at various temperatures, this study aimed to investigate the extent to which thermal treatment influences the quality and characteristics of the resulting TiO_2 [28].

As shown in Figure 3, the TiO_2 powders exhibited a noticeable color change with increasing calcination temperature, and exhibited a progressive whitening with increasing calcination temperature. Interestingly, while the overall mass of the samples remained unchanged, the volume of the powders decreased, resulting in a denser appearance. This observation suggests that the calcination process promoted particle densification, where individual particles became more compact and the void spaces between them diminished. The reduction in porosity is consistent with enhanced crystallite ordering (section of 3.6), indicating that higher calcination temperatures not only improved structural packing but also facilitated the transition from amorphous to more crystalline phases [29]. Such densification and crystallinity enhancement are crucial parameters, as they directly influence the physicochemical properties of TiO_2, including surface area, stability, and potential performance in photocatalytic and energy conversion applications.

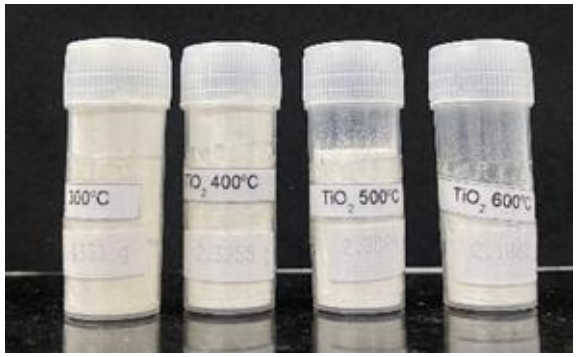

Figure 3: Visual appearance of TiO_2 powders synthesized via green synthesis using CELEs after calcination at different temperatures.

3.3 *Particle Size Analysis (PSA) results*

The particle size distribution of TiO_2–CELEs nanoparticles, presented in Figure 4, shows a dominant peak in the 300–400 nm range with a z–average of 342.6 nm. The cumulative curve indicates that nearly all particles are smaller than 1000 nm, indicating a relatively narrow size distribution. This is further supported by the polydispersity index (PDI) of 0.340, which reflects a stable and moderately uniform dispersion. Collectively, these findings confirm that the green synthesis route effectively produced TiO_2–CELEs nanoparticles within the nanometer scale prior to calcination.

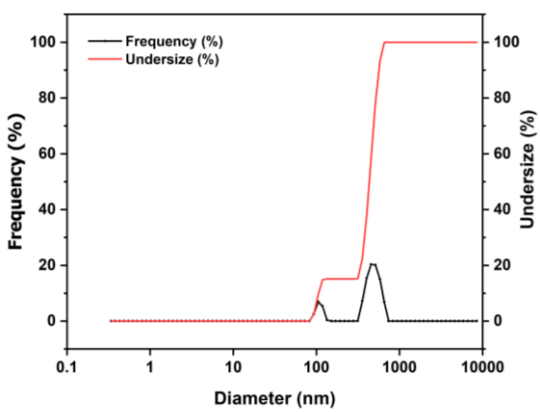

Figure 4: PSA particle size distribution profile.

3.4 *FTIR characterization of TiO_2 NPs*

FTIR analysis was performed to identify the functional groups present in the synthesized TiO_2–CELEs nanoparticles. As shown in Figure 5, the FTIR spectrum exhibited an absorption band at 492 cm^{-1}, corresponding to the Ti–O–Ti vibration characteristic of the TiO_2 structure. The band at 1626 cm^{-1} is associated with H–O–H bending vibrations, indicating the presence of adsorbed water molecules on the TiO_2 surface [3]. A weak band near 2350 cm^{-1} can be attributed to the asymmetric stretching vibration of carbon dioxide (CO_2) molecules adsorbed on the TiO_2 surface. This peak commonly appears as a result of atmospheric CO_2 interacting with surface-active sites of the catalyst [19].

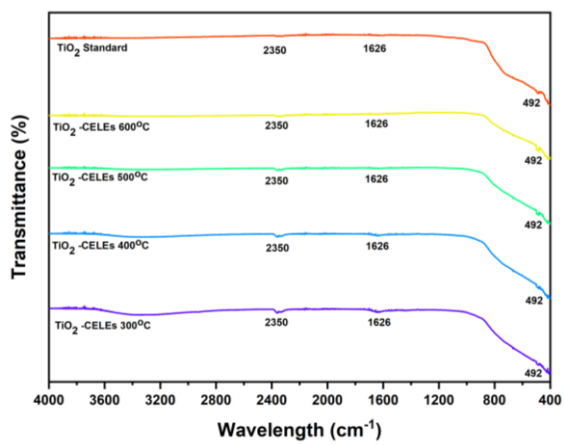

Figure 5: FT–IR spectra of green synthesized TiO_2–CELEs nanoparticles at various calcination temperatures.

In this study, the intensity of the band at 1626 cm^{-1} progressively decreased with increasing calcination temperature, becoming undetectable at 500 and 600 °C. This indicates that high–temperature treatment effectively removes water molecules adsorbed on the TiO_2 surface. Similarly, the band at 2350 cm^{-1}, which was still evident in the standard and low–temperature samples, gradually weakened at higher temperatures and nearly disappeared at 500 and 600 °C. These changes, as illustrated in Figure 5, suggest that the calcination process also facilitates the removal of CO_2 molecules adsorbed on the surface. Furthermore, XRD results (Figure 6**)** showed no new diffraction peaks or phase transition within the 300–600 °C range, confirming that the TiO_2 lattice remained structurally stable. These findings collectively indicate that the FTIR intensity decrease at 1626 cm^{-1} is mainly due to dehydration and surface cleaning rather than a structural modification of TiO_2.

3.5 *XRD characterization of TiO_2–CELEs Nanoparticles*

XRD analysis was performed using Cu–Kα radiation in the 2θ range of 10°–90°. The overall results of this characterization were used to interpret the overall research, while the crystallite size was determined using the *Debye–Scherrer* equation. As shown in Figure 6, samples calcined at intermediate temperatures (400–500 °C) exhibited distinct diffraction peaks at 2θ ≈ 25.3°, 37.8°, 48.0°, 54.0°, and 62.7°, which correspond to the (101), (004), (200), (105), (211) and (204) planes of the anatase TiO_2 phase (JCPDS No. 21–1272). The absence of any rutile peaks even at 600 °C suggests that the anatase phase remains thermally stable within this temperature range, likely due to particle size effects or the stabilizing influence of residual surface species derived from the plant extract.

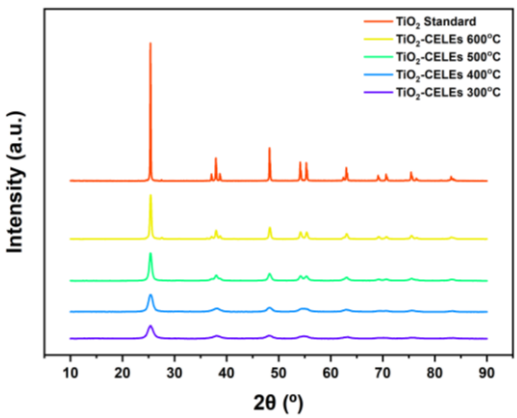

Figure 6: XRD pattern of green-synthesized TiO_2 NPs at different calcination temperatures.

Table 2: Crystal size and crystallinity based on the Scherrer equation.

Material	Crystal Size (nm)	Crystallinity
TiO_2 Standard	35.82	88.30%
TiO_2–CELEs 300 ºC	5.22	71.50%
TiO_2–CELEs 400 ºC	6.33	78.10%
TiO_2–CELEs 500 ºC	10.02	82.80%
TiO_2–CELEs 600 ºC	18.11	80.90%

As shown in Table 2, the crystallite size determined by XRD increased with calcination temperature, from 5.22 nm at 300 °C to 18.11 nm at 600 °C, along with an increase in crystallinity from 71.50% to 82.80%. Before calcination, PSA analysis revealed submicron particle sizes (≈342.6 nm) due to nanoparticle aggregation in the colloidal suspension. In contrast, XRD after calcination reflected the size of individual nanocrystallites.

3.6 *DRS characterization of TiO_2 NPs*

The optical properties of TiO_2 nanoparticles, analyzed by UV–Visible DRS (Figure 7), were strongly influenced by calcination temperature. All samples exhibited strong absorption below 400 nm, typical of TiO_2 semiconductors. Increasing calcination temperature induced a red shift in the absorption edge, indicating reduced band gap energy, while reflectance increased above 400 nm due to particle growth.

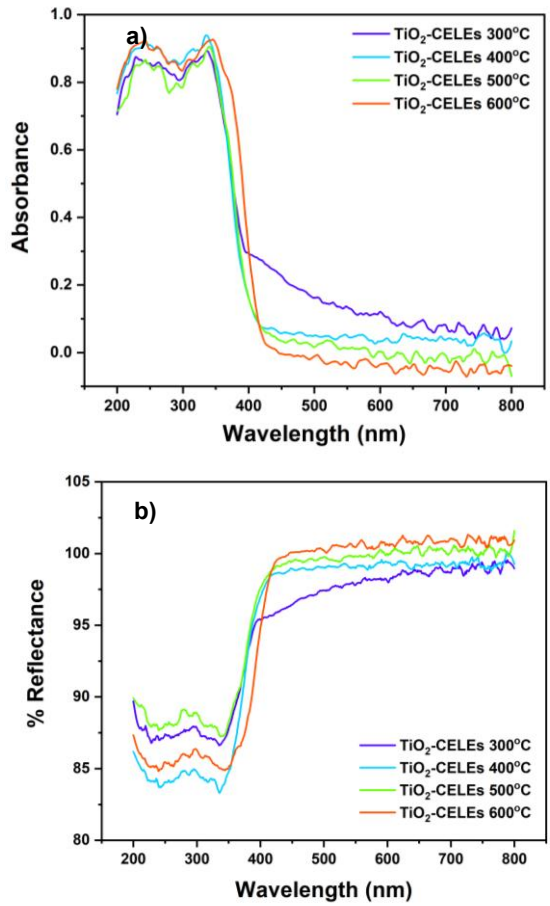

Figure 7: UV–Visible (a) absorbance and (b) reflectance profiles of TiO_2–CELEs nanoparticles.

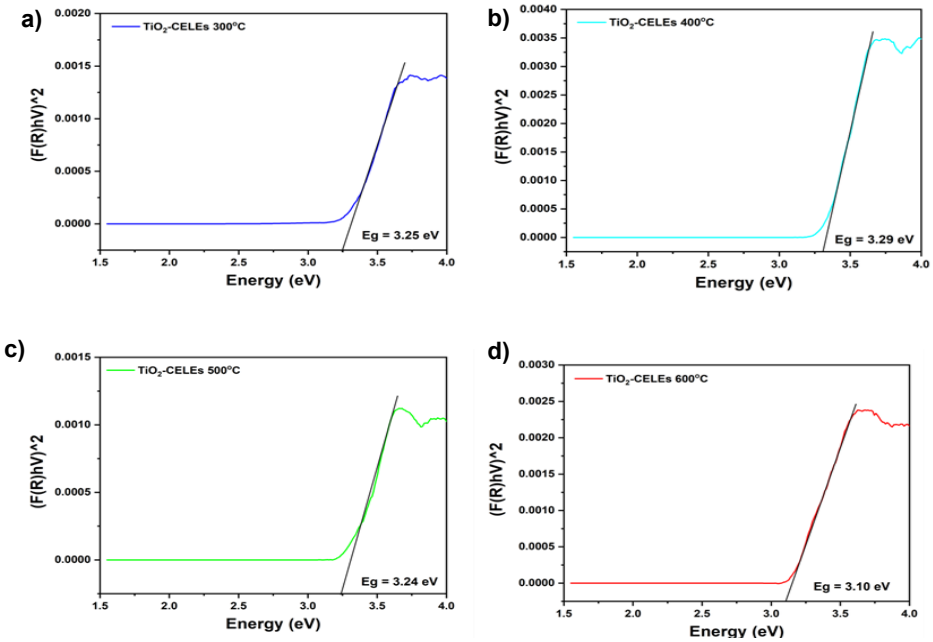

Figure 8: Tauc plot and absorbance spectrum of TiO_2–CELEs Nanoparticles at different temperature: (a) 300 °C, (b) 400 °C, (c) 500 °C, and (d) 600 °C.

The band gap energy of TiO_2 nanoparticles was estimated from UV–Visible DRS using Tauc plot analysis. As shown in Figure 8, the band gap decreased with increasing calcination temperature, from 3.25 eV at 300 °C to 3.10 eV at 600 °C. This trend supports the occurrence of an anatase–to–rutile phase transition at elevated temperatures, consistent with the narrower band gap and stronger reflectivity of rutile compared to anatase. These results highlight the crucial role of calcination temperature in tuning the optical properties of TiO_2 nanoparticles through particle growth and phase transformation.

Thus, the PSA and XRD results complement each other in illustrating the physical transformation of TiO_2–CELEs aggregated colloidal particles to more ordered crystalline structures after calcination. Among all samples, TiO_2–CELEs 500 showed the highest crystallinity (82.80%) with a moderate crystallite size (10.02 nm), indicating that calcination at 500 °C produces a more ordered and structurally stable TiO_2 structure with potentially improved photocatalytic performance.

3.7 *Surface morphology and elemental composition of TiO_2 nanoparticles*

The surface morphology and particle size distribution of the synthesized TiO_2 nanoparticles were examined using scanning electron microscopy (SEM). This technique provided direct visualization of particle shape and aggregation behavior, complementing the structural information obtained from XRD. Figure 9 shows the typical nanosphere morphology of TiO_2–CELEs nanoparticles with a tendency to form aggregates, which varies with calcination temperature (300–600 °C). At 300 °C, the particles appear relatively large (≈116 nm) due to the loss of agglomeration of small crystallites. However, as the temperature increased up to 600 °C, the particle size decreased to the range of 44–58 nm. This decrease in particle size with increasing temperature seems counterintuitive, as calcination typically promotes sintering and particle growth. However, similar observations have been reported in several studies, particularly in systems synthesized via green routes or plant–extract–assisted methods [30]. Such behavior is often attributed to the decomposition of organic capping agents and the release of surface–adsorbed species, which facilitate the breakdown of large aggregates into smaller, more crystalline domains [31].

This variation in particle size suggests morphological restructuring induced by thermal energy, where initially agglomerated particles undergo a process of reorganization and aggregate disintegration, resulting in more uniform particles, particularly at 300–500 °C. Such morphological

changes are highly relevant to photocatalytic applications, as smaller and more homogeneous particles can enhance surface area and improve light absorption efficiency. Consequently, TiO_2–CELEs nanoparticles with reduced size and higher uniformity are expected to exhibit superior photocatalytic activity in degradation processes, since more active sites become available for pollutant adsorption and subsequent photodegradation reactions [32]–[34]. In addition, EDS analysis, as shown in Figure 10. confirmed that the EDS spectrum of TiO_2–CELEs nanoparticles shows dominant peaks corresponding to Titanium (Ti K) and Oxygen (O K). The notation "K" refers to the characteristic X–ray line associated with electron transitions to the K–shell of each element—electrons from outer orbitals fall into the K–shell, emitting X–ray radiation detected by the EDS system [35], [36]. Therefore, "K" does not indicate potassium, but rather the K–line of the element. The dominant peaks in the EDS spectrum were Ti and O, while minor signals appeared as small peaks or background features[37].

According to Table 3, the EDS results confirmed the presence of titanium (Ti) and oxygen (O) as the main elements in all samples, with their proportions changing depending on calcination temperature. At ideal conditions, TiO_2 has a Ti/O ratio of 0.5, reflecting a stable oxide structure.

Table 3: Elemental composition and Ti/O ratio of TiO_2 samples at various calcination temperatures.

Materials	Atom (%at)		Weight (%wt)		Ratio
	Ti K	O K	Ti K	O K	(Ti/O)
TiO_2 Standard	42.18	57.82	68.59	31.41	0.73
TiO_2-CELEs 300 °C	31.27	68.73	57.66	42.34	0.45
TiO_2-CELEs 400 °C	41.89	58.11	68.34	31.66	0.72
TiO_2-CELEs 500 °C	63.12	36.88	83.67	16.33	1.71
TiO_2-CELEs 600 °C	33.97	66.03	60.64	39.36	0.51

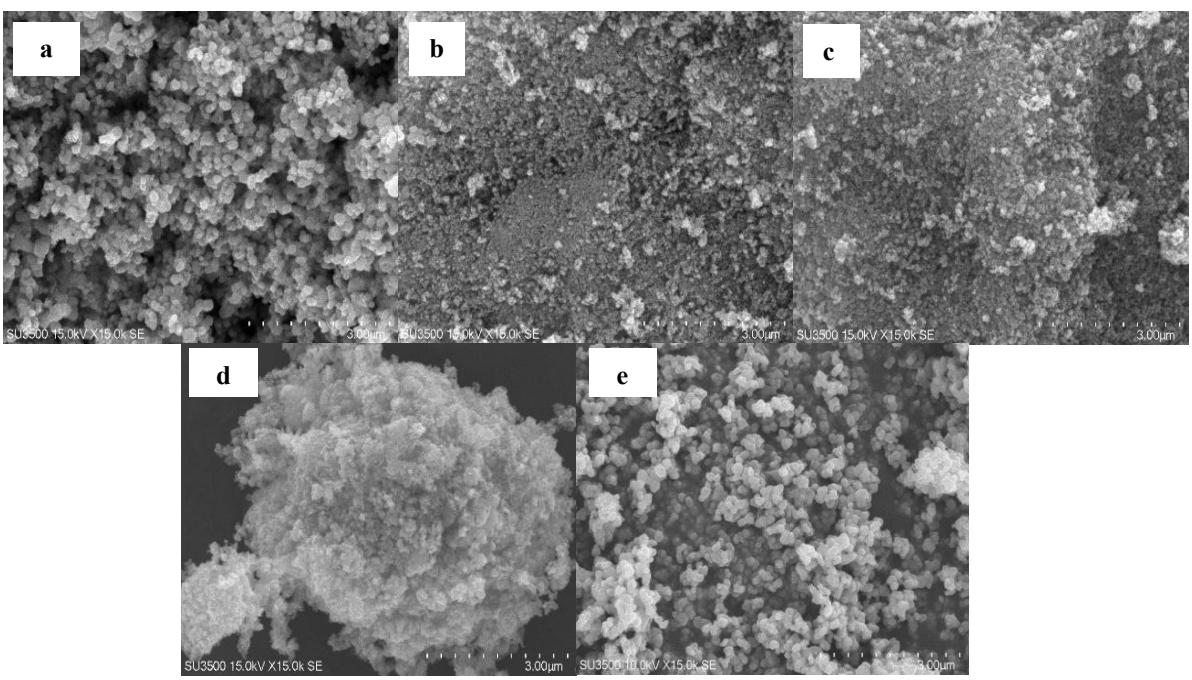

Figure 9: Morphology of TiO_2–CELEs nanoparticles calcined at different temperatures: (a) 300 °C, (b) 400 °C, (c) 500 °C, (d) 600 °C, and (e) TiO_2 standard.

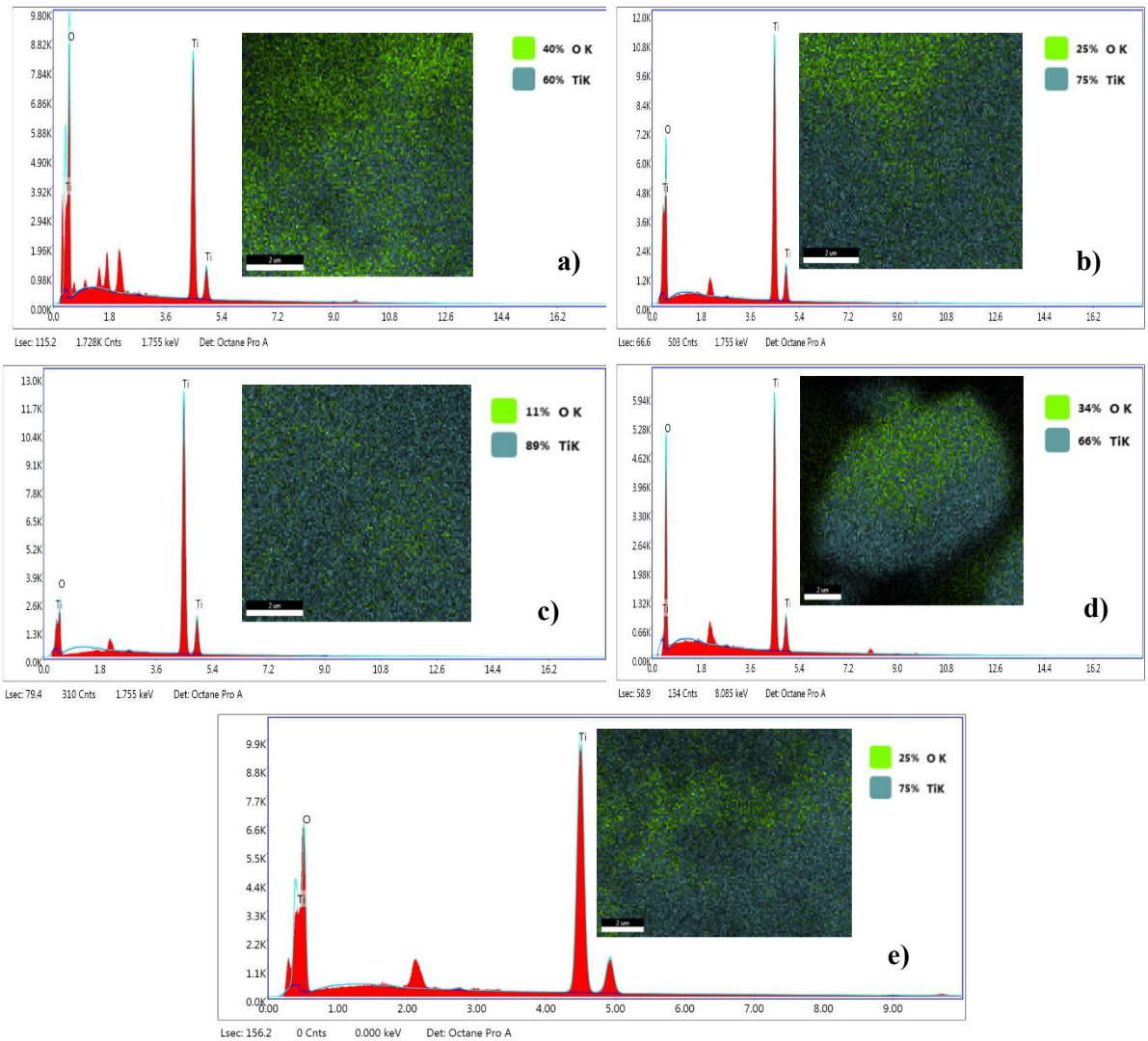

Figure 10: Energy–dispersive X–ray spectroscopy (EDS) spectra of TiO_2–based samples: (a) TiO_2–CELEs calcined at 300 °C, (b) 400 °C, (c) 500 °C, and (d) TiO_2 standard.

At 500 °C, however, the ratio sharply increased to 1.71, showing oxygen loss and the formation of vacancies that can trap electrons and boost charge separation. When heated to 600 °C, the ratio slightly returned toward normal (0.51), likely due to reoxidation on the surface. Overall, the calcination temperature governs the balance between structural stability and defect formation, where TiO_2–CELEs 400°C exhibits greater structural stability, while TiO_2–CELEs 500 °C develops a slight oxygen deficiency that enhances its photocatalytic performance.

3.8 *Specific surface area and pore properties of TiO_2*

The BET results indicate that calcination temperature significantly alters the textural properties of TiO_2. As shown in Table 4, the specific surface area of TiO_2 is strongly influenced by the calcination temperature. The standard TiO_2 exhibited a low SBET (8.38 m^2/g) with small porosity, whereas treatment at 300–400 °C resulted in a significant increase up to 84.94–106.31 m^2/g with an average pore diameter of around 6.5 nm.

This indicates the formation of a mesoporous structure that provides a larger contact area and more active sites.

In addition to influencing Ti/O stoichiometry, calcination temperature also affected the textural properties of TiO_2. At 400 °C, the sample exhibited a high surface area, indicating well–dispersed nanoparticles with stable stoichiometry. However, at higher temperatures (500–600 °C), the surface area drastically decreased (60.13–33.09 m^2/g) due to grain growth and sintering, although the pore diameter increased to around 28 nm. These changes directly impact photocatalytic and DSSC performance, as a higher surface area facilitates dye or pollutant adsorption, while moderate oxygen vacancies at 500 °C enhance charge separation and light–harvesting efficiency. Overall, TiO_2–CELEs calcined at 400–500 °C offer an optimal balance between structural stability, surface reactivity, and photocatalytic potential.

Capillary condensation during adsorption may also become less stable upon desorption, resulting in an apparently higher desorption volume. Minor experimental fluctuations, including slight variations in temperature, pressure, or degassing procedures, might further contribute to this behavior [38].

Table 4: BET surface area and pore volume of TiO_2 samples.

Materials	S_{BET} (m^2/g)	Vp (cm^3/g)	Dp (nm)
TiO_2 Standard	8.38	0.02	3.06
TiO_2–CELEs 300 °C	84.94	0.41	6.50
TiO_2–CELEs 400 °C	106.31	0.24	6.52
TiO_2–CELEs 500 °C	60.13	0.39	6.52
TiO_2–CELEs 600 °C	33.09	0.24	28.48

Among the samples, TiO_2–CELEs 400 °C is emphasized because it exhibits the highest specific surface area (SBET = 106.31 m^2/g), providing the most accessible mesoporous network for gas interactions and thus serving as a representative case for discussing the structural and functional implications of this unusual adsorption–desorption behavior.

As shown in Figure 11, the desorption characteristics and surface textural properties play a decisive role in photocatalytic performance. Extended retention of reactant molecules within mesopores enhances their interaction with TiO_2 active sites, facilitating surface redox reactions under illumination. The TiO_2–CELEs 400 °C sample, with its large surface area and well–developed mesoporosity,

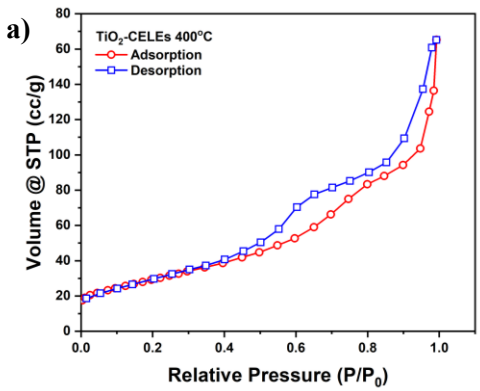

pro abundant adsorption sites that promote efficient reactant diffusion and light absorption. Nevertheless, a high surface area alone is insufficient for superior photocatalytic performance, which is ultimately governed by a balance between surface accessibility and charge carrier dynamics. In contrast, as discussed in Section 3.6, TiO_2–CELEs 500 °C exhibits higher crystallinity, which improves charge separation and electron mobility.

Figure 11: BET Adsorption–Desorption Isotherm Curve of TiO_2–CELEs: a) 400 °C and b) 500 °C.

3.9 *Comparison with previously reported green-synthesized TiO_2*

Plant–assisted synthesis successfully promotes stable TiO_2 structures under moderate calcination, as demonstrated by the comparison of TiO_2 nanoparticles synthesized using different plant extracts (Table 5), which primarily form the anatase phase. The phytochemical composition and calcination temperature have a significant impact on the crystallite sizes, which range from 5.8 to 140 nm. The nanoscale sizes (6.33–10.02 nm) of the TiO_2–CELEs samples in this study are similar to those of phenolic–rich plants

like *Syzygium* cumini and *Amaranthus tricolor*, suggesting that metabolites in *Colocasia esculenta* L. leaves efficiently stabilize particle growth during calcination.

Green-synthesized TiO_2 usually has optical band gaps between 2.51 and 3.48 eV. Like pure anatase TiO_2, TiO_2–CELEs exhibits values of 3.29 eV (400 °C) and 3.24 eV (500 °C), with a slight decrease with temperature, indicating enhanced crystallinity and charge transport. Overall, TiO_2–CELEs 500 °C exhibits a narrow band gap (3.24 eV), moderate crystallite size (10.02 nm), and high crystallinity (82.8%), confirming the extract's role as an eco–friendly and reliable biotemplate for the controlled synthesis of high–crystallinity anatase TiO_2 nanoparticles.

Table 5: Characteristic TiO_2 nanoparticles from different plant extracts and calcination temperatures.

Plant Source	Calcination Temp. and Time	Crystal Size (nm)	Band Gap (eV)	Ref
Jatropha curcas L.	450 °C, 3 h	13	3.28	[4]
Orange peel	500 °C, 4 h	21.61	2.51	[10]
Mentha arvensis	500 °C, 3 h	20–70	–	[18]
Red spinach *(Amaranthus Tricolor* L.)	500 °C, 3h	10.67	2.98–3.00	[19]
Syzygium cumini	570 °C, 3 h	10	3.48	[39]
Citrus limetta	550 °C, 2 h	80–100	3.22	[40]
Lemon peel	500 °C, 2 h	80–140	3.08	[41]
Impatiens rothii Hook.*f.*	500 °C, 3 h	11–25	3.39	[42]
Colocasia esculenta L.: a. TiO_2–CELEs 400 °C	400 °C, 3 h	6.33	3.29	This work
b. TiO_2–CELEs 500 °C	500 °C, 3 h	10.02	3.24	This work

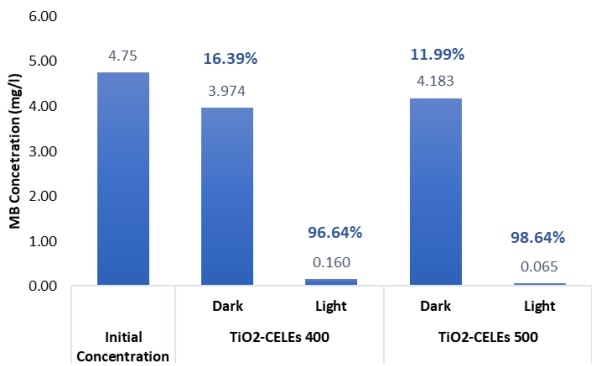

Figure 12: Photodegradation test of methylene blue (5 mg/L) using TiO_2 nanoparticles for 1 hour under dark and light conditions.

3.10 *Photocatalytic degradation of methylene blue*

The methylene blue degradation test (Figure 12) highlights how calcination temperature influences TiO_2 performance. TiO_2–400 °C, with its larger surface area (106.31 m^2/g) and smaller crystal size (6.33 nm), adsorbed more dye molecules (16.39%) even in the dark, as supported by its high pore volume in the isotherm curve. Despite slightly lower crystallinity (78.1%), it still achieved strong photodegradation efficiency (96.64%) due to abundant active sites.

Meanwhile, TiO_2–500 °C exhibited a smaller surface area (60.13 m^2/g) and a larger crystallite size (10.02 nm), which led to reduced adsorption capacity (11.99%). However, its higher crystallinity (82.8%) played a dominant role in enhancing photocatalytic performance by facilitating more efficient charge separation and reducing electron–hole recombination, leading to a superior degradation efficiency (98.64%).

Overall, these results demonstrate that, despite its lower surface area, TiO_2–CELEs 500 °C exhibits better photocatalytic activity primarily due to its higher crystallinity. This indicates that crystalline order has a more significant impact than surface area in governing the photocatalytic efficiency under the studied conditions.

4 Conclusions

TiO_2 nanoparticles were successfully synthesized via a green approach using *Colocasia esculenta* L. leaf extract (CELEs) as a bioreducing and stabilizing agent, followed by calcination at 300–600 °C. Calcination temperature exerted a pronounced effect on both the structural and functional characteristics of the materials. TiO_2–CELEs 400 °C exhibited the highest specific surface area (106.31 m^2/g) and the smallest crystallite size (6.33 nm), favoring enhanced adsorption. In contrast, TiO_2–CELEs 500 °C showed the highest crystallinity (82.8%) and achieved the

highest photocatalytic efficiency toward methylene blue degradation (98.64%). These results reveal a clear trade-off between surface area and crystallinity, with moderate calcination (≈450–500 °C) offering the optimal compromise between surface reactivity and charge separation efficiency. The utilization of CELEs as a local, renewable phytochemical precursor thus provides a sustainable and low-cost pathway for producing high-performance TiO_2 nanomaterials applicable to photocatalysis and dye-sensitized solar cells.

Acknowledgments

This research was financially supported by Directorate of Research and Community Service, Ministry of Education, Culture, Research, and Technology of the Republic of Indonesia (Contract Number: 007/LPPM-UP/KPFR/VI/2025 and 7928/LL4/PG/2025).

Author Contributions

L.J.K.: research design, investigation, writing an original draft, and editing; IPM.: conceptualization, data curation, writing—reviewing and editing. N.N.: conceptualization, data analysis and review; T.S.H.: investigation, methodology. APW: investigation, data processing, and validation. AI: reviewing and editing. All authors have read and agreed to the published version of the manuscript.

Conflicts of Interest

The authors declare no conflict of interest.

Declaration of generative AI and AI-assisted technologies in the writing process

The authors utilized the ChatGPT tool to enhance the language and readability of the manuscript.

References

[1] G. Zhang, A. Song, Y. Duan, and S. Zheng, "Enhanced photocatalytic activity of TiO_2/zeolite composite for abatement of pollutants," *Microporous and Mesoporous Materials*, vol. 255, pp. 61–68, 2018, doi: 10.1016/j.micromeso.2017.07.028.

[2] S. H. S. Okto and Munasir, "Review: Green synthesis TiO_2 nanoparticle as photocatalyst material," *Jurnal Inovasi Fisika Indonesia*, vol. 2, no. 12, p. 82, 2023.

[3] L. J. Kusumawardani and Y. Syahputri, "Study of structural and optical properties of Fe(III)-doped TiO_2 prepared by sol-gel method," in *IOP Conference Series: Earth and Environmental Science*, Bristol, UK: Institute of Physics Publishing, Jul. 2019, doi: 10.1088/1755-1315/299/1/012066.

[4] S. P. Goutam, G. Saxena, V. Singh, A. K. Yadav, R. N. Bharagava, and K. B. Thapa, "Green synthesis of TiO_2 nanoparticles using leaf extract of *Jatropha curcas* L. for photocatalytic degradation of tannery wastewater," *Chemical Engineering Journal*, vol. 336, pp. 386–396, Mar. 2018, doi: 10.1016/j.cej.2017.12.029.

[5] I. Fatimah, A. Said, and U. A. Hasanah, "Preparation of TiO_2-SiO_2 using rice husk ash as silica source and the kinetics study as photocatalyst in methyl violet decolorization," *Bulletin of Chemical Reaction Engineering and Catalysis*, vol. 10, no. 1, pp. 43–49, Apr. 2015, doi: 10.9767/bcrec.10.1.7218.43-49.

[6] A. M. Riska and N. P. Putri, "Green synthesis TiO_2 Menggunakan Ekstrak Daun Pepaya (*Carica Papaya* L.) sebagai Bioreduktor yang Berpotensi dalam Aplikasi Fotokatalitik green synthesis of TiO_2 using Papaya (*Carica papaya* L.) leaf extract as a bioreductor with potential in photocatalytic applications," *Sains dan Matematika*, vol. 9, no. 1, pp. 1–7, 2024.

[7] T. Pushpamalini, M. Keerthana, R. Sangavi, A. Nagaraj, and P. Kamaraj, "Comparative analysis of green synthesis of TiO_2 nanoparticles using four different leaf extract," *Materials Today: Proceedings*, vol. 40, 2020, pp. S180–S184, doi: 10.1016/j.matpr.2020.08.438.

[8] I. Nuhaeroh, D. I. Anwar, and L. L. Khumaisah, "Antibacterial activity of TiO_2/Cu and TiO_2/CuO nanocomposites against *Bacillus cereus*," *Jurnal Sains Dasar*, vol. 11, no. 2, pp. 95–100, Apr. 2023, doi: 10.21831/jsd.v11i2.53247.

[9] M. D. Dilika, G. M. Fanta, and T. Tański, "Green synthesis of titanium dioxide nanoparticles using *Maerua oblongifolia* root bark extract: Photocatalytic degradation and antibacterial activities," *Materials*, vol. 17, no. 23, Dec. 2024, doi: 10.3390/ma17235835.

[10] A. M. Amanulla and R. Sundaram, "Green synthesis of TiO_2 nanoparticles using orange peel extract for antibacterial, cytotoxicity and humidity sensor applications," *Materials Today: Proceedings*, vol. 8, Part 1, pp. 323–331, 2019, doi: 10.1016/j.matpr.2019.02.118.

[11] L. J. Kusumawardani, A. Iryani, and E. L. Sinaga, "Modification of zeolite made from coal fly ash with TiO_2: Effect of aging time on physical and optical properties," *Makara Journal of Science*, vol. 27, no. 1, Mar. 2023, doi: 10.7454/mss.v27i1.1483.

[12] L. J. Kusumawardani, T. Widyyanti, A. Iryani, U. Hasanah, and N. Nurlela, "Optimization and mechanism elucidation of catalytic photodegradation methylene blue by TiO_2/Zeolite coal fly ash nanocomposite under H_2O_2 presence," *Jurnal Sains Natural*, vol. 14, pp. 98–108, 2024, doi: 10.31938/jsn.v.

[13] I. Prakoso et al., "Photodegradation of methyl orange using TiO_2/zeolite from coal fly ash waste under acidic conditions and H_2O_2 addition," *Helium: Journal of Science and Applied Chemistry*, vol. 4, no. 1, 2024, doi: 10.33751/helium.v4i1.9503.

[14] L. J. Kusumawardani, Y. Syahputri, Apriansyah, and M. Fathurrahman, "TiO_2/zeolite coal fly ash nanocomposite for photodegradation of naphthol blue black dye: optimization and mechanism under visible light," *Jurnal Kimia Valensi*, vol. 11, no. 1, pp. 92–104, May 2025, doi: 10.15408/jkv.v11i1.45036.

[15] A. Panneerselvam, J. Velayutham, and S. Ramasamy, "Green synthesis of TiO_2 nanoparticles prepared from *Phyllanthus niruri* leaf extract for dye adsorption and their isotherm and kinetic studies," *IET Nanobiotechnol*, vol. 15, no. 2, pp. 164–172, Apr. 2021, doi: 10.1049/nbt2.12033.

[16] D. R. Eddy et al., "A review of recent developments in green synthesis of TiO_2 nanoparticles using plant extract: Synthesis, characterization and photocatalytic activity," *Inorganic Chemistry Communications*, vol. 165, Jul. 2024, doi: 10.1016/j.inoche.2024.112531.

[17] R. Oktafianti, N. P. Putri, A. M. Riska, and D. H. Kusumawati, "Degradation performance of methyl orange by TiO_2 photocatalyst from green synthesis," *Journal of Physics: Conference Series*, vol. 2900, 2024, doi: 10.1088/1742-6596/2900/1/012001.

[18] W. Ahmad, K. K. Jaiswal, and S. Soni, "Green synthesis of titanium dioxide (TiO_2) nanoparticles by using *Mentha arvensis* leaves extract and its antimicrobial properties," *Inorganic and Nano-Metal Chemistry*, vol. 50, no. 10, pp. 1032–1038, Oct. 2020, doi: 10.1080/24701556.2020.1732419.

[19] D. Rahmawati et al., "Synthesis of TiO2 nanoparticles using red spinach leaf extract (*Amaranthus Tricolor* L.) for photocatalytic of methylene blue degradation," *Green Chemistry Letters and Reviews*, vol. 17, no. 1, 2024, doi: 10.1080/17518253.2024.2352571.

[20] N. T. H. Simalango, N. M. Puspawati, and I. M. Sukadana, "Investigation of toxic compounds in ethanol extract of taro leaves (*Colocasia esculenta* L.) using the brine shrimp lethality test method," *Jurnal Kimia*, vol. 18, no. 2, p. 99, Aug. 2024, doi: 10.24843/JCHEM.2024.v18.i02.p01.

[21] F. Ferreres et al., "Further knowledge on the phenolic profile of *Colocasia esculenta* L. Shott," *Journal of Agricultural and Food Chemistry*, vol. 60, no. 28, pp. 7005–7015, Jul. 2012, doi: 10.1021/jf301739q.

[22] Y. N. Andarini et al., "Morphological character variability of Javanese local taro (*Colocasia esculenta*) germplasm," *Buletin Plasma Nutfah*, vol. 24, no. 1, pp. 63–76, Oct. 2018, doi: 10.21082/blpn.v24n1.2018.p63-76.

[23] P. Rajaram, A. R. Jeice, and K. Jayakumar, "Influences of calcination temperature on titanium dioxide nanoparticles synthesized using *Averrhoa carambola* leaf extract: *In vitro* antimicrobial activity and UV-light catalyzed degradation of textile wastewater," *Biomass Conversion and Biorefinery*, vol. 14, no. 17, pp. 20665–20678, Sep. 2024, doi: 10.1007/s13399-023-04212-x.

[24] L. J. Kusumawardani and Y. Syahputri, "Study of structural and optical properties of Fe(III)-doped TiO_2 prepared by sol-gel method," *IOP Conference Series: Earth and Environmental Science*, vol. 299, Jul. 2019, doi: 10.1088/1755-1315/299/1/012066.

[25] D. Febriantini, B. Purnomo, U. Lasibunga, and Y. Yulizar, "Controlled fabrication of novel zirconia nanoparticles with tailored size, morphology, crystal phases, surface properties,

and acidity via Indonesian *Boehmeria virgata*-mediated eco-friendly synthesis," *Ceramics International*, vol. 49, no. 22, pp. 34461–34471, Nov. 2023, doi: 10.1016/j.ceramint.2023.08.024.

[26] M. M. Martin and R. E. Sumayao, "Facile green synthesis of silver nanoparticles using *Rubus rosifolius Linn* aqueous fruit extracts and its characterization," *Applied Science and Engineering Progress*, vol. 15, no. 3, Jul. 2022, Art. no. 5511, doi: 10.14416/j.asep.2021.10.011.

[27] Z. Villagrán et al., "Plant-based extracts as reducing, capping, and stabilizing agents for the green synthesis of inorganic nanoparticles," *Resources*, vol. 13, no. 6, 2024, doi: 10.3390/resources13060070.

[28] D. Ayunda et al., "Preparation and characterization of ZnO/TiO_2 nanoparticles using papaya leaf extract," *Media Farmasi Indonesia*, vol. 15, no. 2, 2018, doi: 10.37013/jf.v1i1.65.

[29] D. Febriantini, Purnamasari, A. R. Liandi, Usman, and Y. Yulizar, "A comprehensive study on the influence of single and multiple phytochemicals in facilitating green synthesis of ZrO_2 nanoparticles," *Nano-Structures and Nano-Objects*, vol. 39, Sep. 2024, doi: 10.1016/j.nanoso.2024.101303.

[30] C. Chang, S. Rad, L. Gan, Z. Li, J. Dai, and A. Shahab, "Review of the sol-gel method in preparing nano TiO_2 for advanced oxidation process," *Nanotechnology Reviews*, vol. 12, no. 1, 2023, doi: 10.1515/ntrev-2023-0150.

[31] J. H. F. Chau et al., "Study of Calcination Temperature Influence on Physicochemical Properties and Photodegradation Performance of $Cu_2O/WO_3/TiO_2$," *Catalysts*, vol. 15, no. 6, Jun. 2025, doi: 10.3390/catal15060601.

[32] G. P. Zaragosa, C. N. D. Ilem, and J. Garcia, "Watermelon (*Citrullus lanatus*) rind extract-mediated synthesis of manganese oxide nanoparticles for theranostic applications," *Applied Science and Engineering Progress*, vol. 17, no. 1, Sep. 2024, Art. no. 7329, doi: 10.14416/j.asep.2024.02.002.

[33] N. Shakeel, I. Piwoński, P. Iqbal, and A. Kisielewska, "Green synthesis of titanium dioxide nanoparticles: Physicochemical characterization and applications: A review," *International Journal of Molecular Sciences*, Jun. 2025, doi: 10.3390/ijms26125454.

[34] I. Fatimah et al., "Highly active photocatalyst of nickel oxide nanoparticles green-synthesized using *Tinosphora cordifolia*-plant extract for photocatalytic oxidation of tetracycline," *Environmental Nanotechnology, Monitoring and Management*, vol. 22, Dec. 2024, doi: 10.1016/j.enmm.2024.100968.

[35] L. J. Kusumawardani and A. Iryani, "Photocatalytic degradation of phenol using TiO_2-Fe under H_2O_2 presence by visible and sunlight irradiation," *Jurnal Kimia Valensi*, vol. 7, no. 2, pp. 94–99, Nov. 2021, doi: 10.15408/jkv.v7i2.20766.

[36] D. E. Newbury and N. W. M. Ritchie, "Is scanning electron microscopy/energy dispersive X-ray spectrometry (SEM/EDS) quantitative?," *Scanning*, vol. 35, no. 3, pp. 141–168, May 2013, doi: 10.1002/sca.21041.

[37] A. Arenas-Hernandez et al., "Study of oxygen vacancies in TiO_2 nanostructures and their relationship with photocatalytic activity," *Applied Sciences (Switzerland)*, vol. 12, no. 7, Apr. 2022, doi: 10.3390/app12073690.

[38] M. Fathurrahman, A. Zulys, and J. Gunlazuardi, "Kinetic study and optimization of tetramethylthionine chloride photodegradation by iron-perylene MOF with hydrogen peroxide using response surface methodology," *Applied Science and Engineering Progress*, vol. 18, no. 3, Jul. 2025, Art. no. 7683, doi: 10.14416/j.asep.2025.02.002.

[39] S. H. S. Okto, A. As, A. R. Putri, and M. Basmalah, "Green synthesis TiO_2 nanoparticles using juwet (*Syzygium cumini*) leaf extract as a photocatalytic material for Pb^{2+} ion removal in industrial wastewater," in *Proceedings of the Seminar Nasional UNIMUS*, vol. 5, 2022. [Online]. Available: https://prosiding.unimus.ac.id/index.php/semnas/article/view/1216

[40] G. Nabi, A. Majid, A. Riaz, T. Alharbi, M. A. Kamran, and M. Al-Habardi, "Green synthesis of spherical TiO_2 nanoparticles using *Citrus Limetta* extract: Excellent photocatalytic water decontamination agent for RhB dye," *Inorganic Chemistry Communications*, vol. 129, Jul. 2021, doi: 10.1016/j.inoche.2021.108618.

[41] G. Nabi et al., "Green synthesis of TiO_2 nanoparticles using lemon peel extract: their

optical and photocatalytic properties," *International Journal of Environmental Analytical Chemistry*, vol. 102, no. 2, pp. 434–442, 2022, doi: 10.1080/03067319.2020.1722816.

[42] G. B. Yitagesu, D. T. Leku, and G. A. Workneh, "Green synthesis of TiO_2 using impatiens *rothii Hook.f.* leaf extract for efficient removal of methylene blue dye," *ACS Omega*, vol. 8, no. 46, pp. 43999–44012, Nov. 2023, doi: 10.1021/acsomega.3c06142.